Modelling the macroscopic behavior of Strombolian explosions at Erebus volcano

E. de Lauro, S. de Martino, M. Falanga, M. Palo

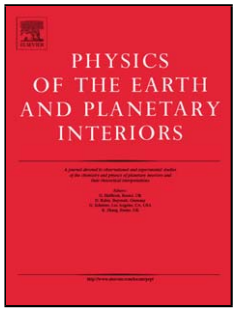

Title: Modelling the macroscopic behavior of Strombolian explosions at Erebus volcano

Authors: E. De Lauro, S. De Martino, M. Falanga, M. Palo

PII: S0031-9201(09)00123-X
DOI: doi:10.1016/j.pepi.2009.05.003
Reference: PEPI 5170

To appear in: *Physics of the Earth and Planetary Interiors*

Received date: 30-10-2008
Revised date: 3-4-2009
Accepted date: 1-5-2009

Please cite this article as: De Lauro, E., De Martino, S., Falanga, M., Palo, M., Modelling the macroscopic behavior of Strombolian explosions at Erebus volcano, *Physics of the Earth and Planetary Interiors* (2008), doi:10.1016/j.pepi.2009.05.003

Modelling the macroscopic behavior of Strombolian explosions at Erebus volcano

E. De Lauro[a], S. De Martino[a,c], M. Falanga[*,b,c], M. Palo[a]

[a] *Dipartimento di Matematica e Informatica, Università di Salerno, Via Ponte Don Melillo, 84084 Fisciano (SA), Italia.*
[b] *Dipartimento di Fisica, Università di Salerno, Via S. Allende, 84081 Baronissi (SA), Italia.*
[c] *INFN, Gruppo collegato di Salerno, Via S. Allende, 84081 Baronissi (SA), Italia.*

Abstract

We analyze seismic signals associated with the Strombolian explosion quakes at Erebus volcano (Antarctica), examining the high-frequency ($> 0.5Hz$) portion of the spectrum. We consider recordings relative to two time periods during the years 2005 and 2006. Cross-correlation analysis allows us to distinguish three classes of events. Spectral properties and polarization analysis provide evidence of a very complex volcanic structure. We conduct analyses to elucidate the macroscopic dynamic system associated with the explosions. The distribution of the times between successive explosion-quakes is exponential, implying a Poissonian process as observed at Stromboli volcano but on a different time scale. The sequence of the occurrence of the explosions can be described by classical intermittency. A coalescence Chandrasekar-Landau mean-field model reproduces gas bubble sizes comparable with those observed at the lava lake surface. Finally, the classical equation for the ascent of gas bubbles is generalized by adding a diffusive process. This model provides ascent velocities depending on the bubble radius: for gas bubbles greater than a few centimeters, variation in ascent velocity due to diffusion becomes negligible and the ascent velocity appears to be governed primarily by buoyancy.

*Corresponding Author. Present Address: Dipartimento di Matematica e Informatica, Università di Salerno, Via Ponte Don Melillo, Fisciano (SA) 84084 Italia. Tel.:+39 089965288; fax: +39 089965275.

Email address: rosfal@sa.infn.it (M. Falanga)

Key words: Strombolian explosions, Erebus volcano, Diffusion.

1. Introduction

A variety of eruption styles can be observed at active volcanoes, and even at the same volcano at different time periods. Among the eruption styles, Strombolian activity is commonly observed at many volcanoes worldwide and its understanding can enlighten the fluid-dynamics system that operates within the magmatic plumbing system. Recent studies have demonstrated some properties of the macroscopic and mesoscopic dynamic system associated with this phenomenon (see, e.g., De Lauro et al. (2008) and references therein) by looking at tremor and explosion-quakes generated by Stromboli volcano (Italy). It is important to verify whether some basic properties such as radiality in the wavefield, low-dimensionality in the source process mechanism, broad-band spectrum, Poissonian occurrence of the explosions can be recognized by looking at other volcanoes in order to extract a general meaning.

In this work, we show results obtained from a study of Erebus volcano (Antarctica), whose continuous monitoring system provides a high-quality data set. Erebus volcano is an active strato-volcano located on Ross Island in the Ross sea (see Fig. 1). Its predominant activity is Strombolian, characterized by the occurrence of 3-4 explosion quakes per day, but a few episodes of phreatic explosions have also occurred in the past thirty years (Aster et al., 2003). Occasionally, swarms of several hundred explosions per day have been observed (Kaminuma, 1987; Rowe et al., 2000). The Strombolian explosions are produced by the bursting of over-pressured gas bubbles having a radius of 3-5 meters. They are visible at the surface of a lava lake, which is the upper part of a shallow magmatic chamber. The convecting lava lake and magma conduit are composed of phonolite (see, e.g., Kyle, 1977; Kyle et al., 1992). Besides the lava lake, other vents can produce eruptions of ash and lava flows. The first recordings of seismic signals at Erebus were obtained in the 1970's (e.g. Giggenbach et al., 1973). Since then, the properties of the seismic and infrasonic wavefields have been studied (e.g. Johnson et al., 2003) looking in particular at the very long period (VLP) signals preceding and following the explosions (Rowe et al., 1998; Aster et al., 2003). The VLP signals at Erebus have been associated with the magma movements induced by gravity or inertial forces, which follow the slug ascent, eruption and recharge of the

lava lake, even though a dynamic model to explain this process has not yet been fully developed.

The preliminary part of this work examines the high-frequency ($> 0.5Hz$) portion of the Strombolian explosion spectrum. We characterize the signals in terms of their frequency content, waveform, polarization properties and energy distribution checking whether already known characteristics of VLPs are also common to the high frequency counterpart. These analyses establish the wavefield properties on the time scale of the explosions' duration.

To get an overall understanding of the explosive process, we study Erebus volcano on a longer time scale, extracting some macroscopic properties such as the rate of the occurrence of the explosions and the low dimensional dynamic system associated with them (Konstantinou, 2002). In fact, a signature of the Strombolian activity is the Poissonian occurrence of the explosions (Bottiglieri et al., 2005). Therefore, we study the times between successive explosions, comparing the results with those from Stromboli. A simple diffusive model producing slugs from a permanent degassing source has been conjectured for Stromboli (Bottiglieri et al., 2005): It provides the sizes of the exploding gas bubbles. Apparently, at Erebus, the formation of large bubbles and the absence of a persistent tremor could require modification of this approach. Nevertheless, we suggest that a permanent flux in a cavity produces cavity vibrations (tremor) only if there is a suitable impingement geometry and, at low Reynolds numbers, the convective scales match the viscous ones (Villermaux and Hopfinger, 1994; Maurel et al., 1996). In other words, the absence of persistent tremor does not imply the absence of a permanent degassing source. In any case, tremor signals could occur beneath the sensitivity threshold given by the ambient background noise.
Finally, we generalize the classical ascent gas bubble equation by introducing a diffusive term.

2. Data set

Mount Erebus Volcano Observatory (MEVO) provides systematic observations and studies of the nature of the seismic signals of Erebus. Our data set is composed of seismic and infrasonic signals recorded in two time periods: 7th - 28th February 2005 and 26th February - 27th April 2006. The broadband seismic stations are equipped with three-component seismometers (Guralp CMG 40-T), with a linear response in the range 30s-50Hz; the infrasonic signals are recorded by microphones providing data in the frequency

range 20s-20Hz (Aster et al., 2004). Both data sets are sampled at 40 Hz. The seismic stations are E1S, NKB, CON, and LEH; the two infrasonic sensors are located at the stations E1S and NKB. Additional details on the seismic stations and the infrasonic sensors can be found in, e.g., Aster et al. (2004). During 7th - 28th February 2005, 54 explosions occurred, whereas 220 explosions were recorded during 26th February - 27th April 2006. The permanent MEVO short-period and broadband seismic network, and the temporary PASSCAL deployments are indicated in Fig. 1.

During 2006 we have only the seismic recordings from E1S, which are the only free-accessible on the IRIS web-site. To avoid analyzing the ice-quakes, we have checked the occurrence times of the explosions with the catalog reported at the MEVO website (http://erebus.nmt.edu/). All the seismic signals have been high-pass-filtered with a corner frequency of 0.5 Hz. They last between 15 and 30 s and show a variety of waveforms.

3. Waveform Analysis

The analysis of waveform similarity can be a useful approach to identify a common source mechanism. In particular, at Erebus, Shibuya et al. (1989) recognized a variety of waveforms. On the other hand, by an empirical comparison of different explosion signals, Rowe et al. (2000) showed that they can be a superposition of multiple nearly identical explosion events overlapping with different time lags and amplitude ratios. It is thus appropriate to make a preliminary quantitative analysis of the degree of similarity among the waveforms of our data set. This is done by considering the cross-correlation between the explosions. The analysis is performed first by considering the catalogs of 2005 and 2006 separately, and second by comparing both to each other. Each explosion is selected as a reference event and cross-correlated with all others. Specifically, we compare all the explosions along their entire duration, i.e. using time windows of 40 s from the onset. The cross-correlation functions between all the pairs of events are determined. These functions display the same behavior for all pairs. A representative curve from the 2005 catalog is shown in Fig. 2a: One observes very high correlation coefficients up to the 30th event with one reference event (squared line) and, at the same time, low correlation coefficients with another reference event (line with stars); starting from 30th event the rule is inverted. The high correlation coefficients (> 0.7) indicate two classes of

events that appear clustered in time. Specifically, the first class occurs in *one* day, putting in light a non-stationary phase of the Erebus activity.

An example of the results from 2006 is reported in Fig. 2b. Once again, we recognize two different classes: a reference event is highly correlated with many others (line with stars), while another reference event is completely uncorrelated (dotted line). Additionally, the correlated events show high correlation values with the second class of 2005. Figs. 3a-c show that the stations NKB, LEH, CON display the same clustering as for E1S.

Summarizing, we find evidence for three classes of events so partitioned:

- 2005: 55% of the first class and 45% of the second class
- 2006: 75% of second class and 25% of the third class.

Fig. 4 illustrates some examples from these three classes of events. The third class is characterized by events that are mostly uncorrelated. These explosions could be superimposed signals from multiple events of the other classes as suggested by Rowe et al. (2000). The application of the Independent Component Analysis, a nonlinear deconvolution analysis in the time domain based on fourth-order statistics, does not yield any decomposition as in the case of irreducible systems (De Lauro et al., 2005, 2008).

4. Energy distribution

The energy of the volcanic explosion quakes is difficult to determine due to their emergent onset and the absence of distinct phases. However, it is possible to estimate a quantity proportional to the seismic energy (ε, hereafter): The integral of the square of the signal in the time domain (De Martino et al., 2004; Rowe et al., 2004). We perform a Hilbert transform to obtain the envelope of the seismic signals and we integrate the square of this envelope. The bounds of integration are inferred from the signal-to-noise ratio (SNR). Specifically, the bounds of integration are selected by considering the first peaks (preceding and following the maximum amplitude of each explosion) with amplitudes equal to the noise level (the level of noise is equal to 0.3 μ m/s within 20%). The quantity thus obtained is proportional to the seismic energy of the explosion quakes. Our estimate is made considering the explosions recorded at the station nearest to the lava lake (E1S) and by using the radial component of the motion.

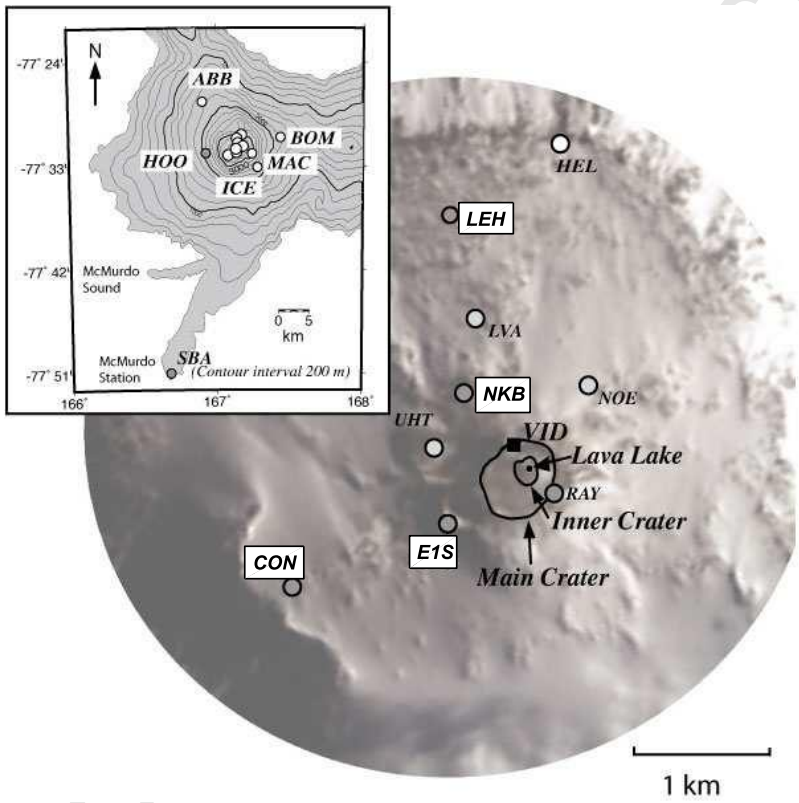

Figure 1: Map of Ross Island showing the location of the permanent MEVO short-period and broadband seismic network, and the temporary PASSCAL deployments (extracted from MEVO web site http://erebus.nmt.edu). The stations selected for our work are labelled by a box (E1S, NKB, CON, LEH).

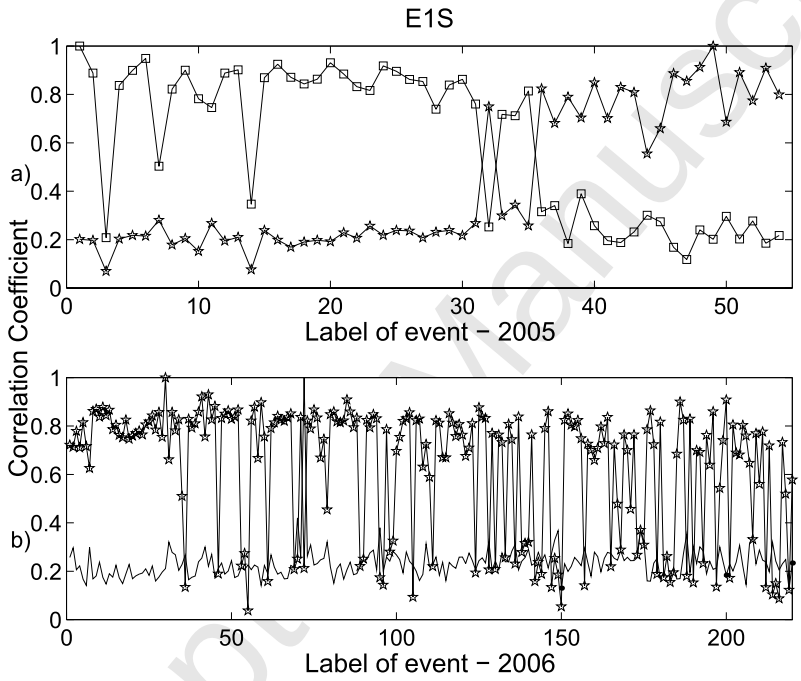

Figure 2: Cross-correlation curves between two reference events and all the other explosions at E1S in 2005 and 2006 respectively: a) The squared-curve indicates the cross-correlation values with respect to the reference event recorded on 07/02/2005 h 05:51:01 UT, whereas the star curve is relative to another reference event (27/02/2005 h 14:11:09 UT); b) The stars show the events cross-correlated with the reference event recorded on 10/03/2006 h 10:47:49 UT and the black circles represent the correlation with another reference event (24/03/2006 h 05:58:23 UT). Notice that the increasing event number corresponds to increasing time.

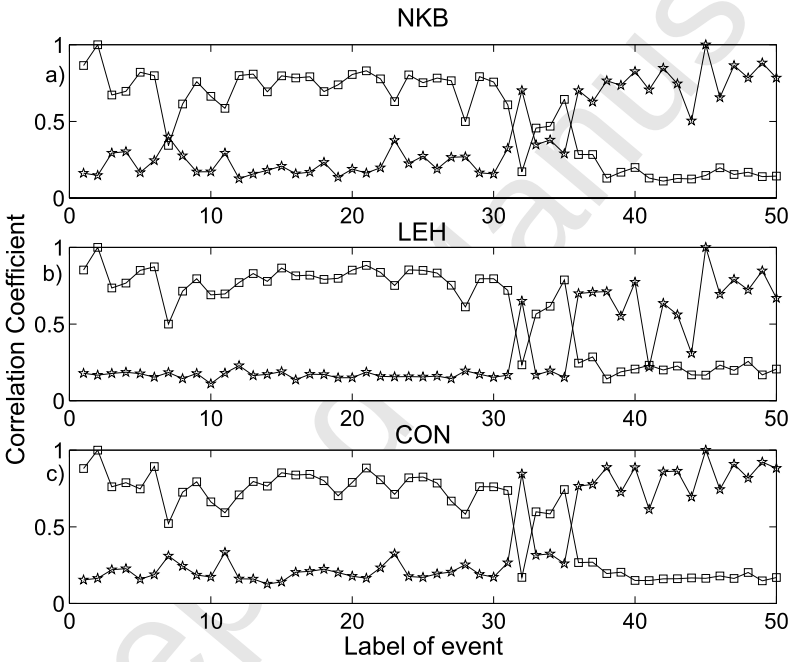

Figure 3: Cross-correlation curves between two reference events and all other explosions at a) NKB, b) LEH, and c) CON in 2005. The squared curve indicates the cross-correlation values with respect to the reference event recorded on 07/02/2005 h 05:51:01 UT, whereas the stars curve is relative to another reference event (27/02/2005 h 14:11:09 UT).

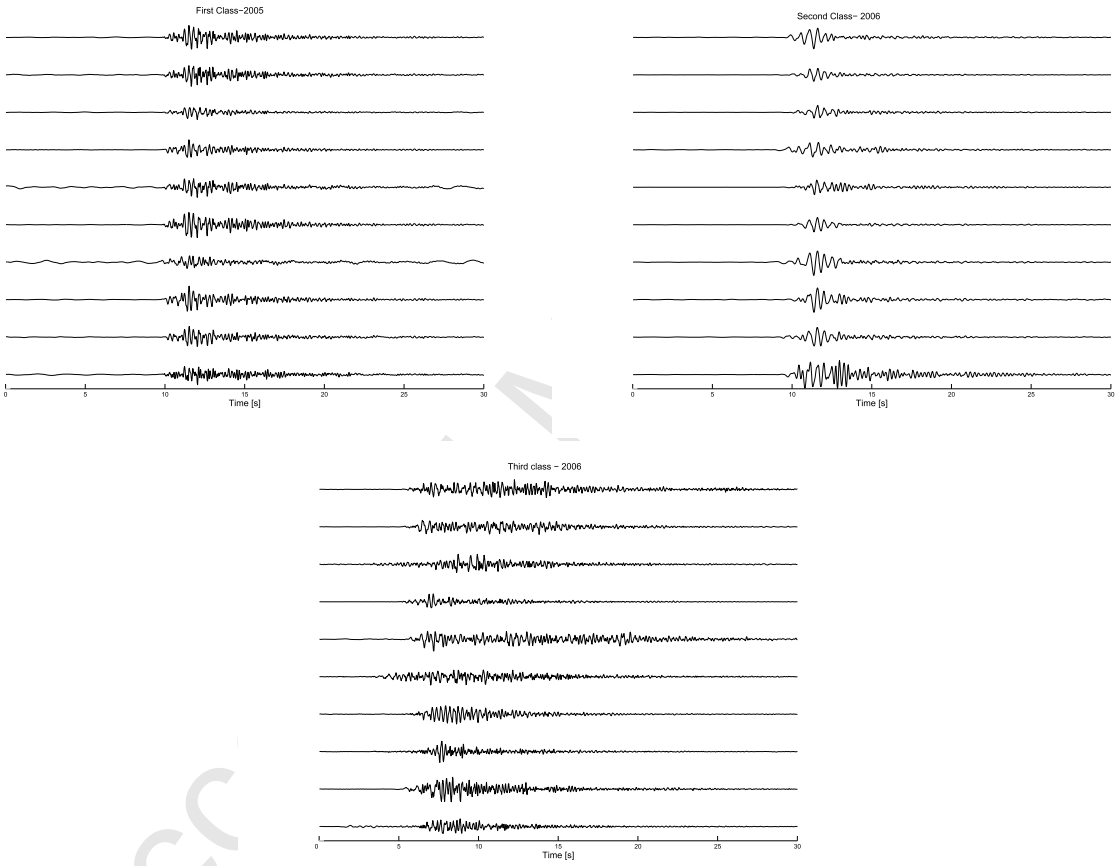

Figure 4: Representative waveforms of the three characteristic classes of the high-frequency filtered radial component recorded at E1S: a) first class; b) second class; c) third class. Note the difference in waveforms within the third class.

The results for the event number of 2005 are reported in Fig. 5. We plot the estimated energies (logarithmic scale) as function of the event number. This procedure allows us to observe the time release of energy. The values of energy span over two orders of magnitude. The clustering in time indicated by waveform analysis is here confirmed by the different mean energy value between the first thirty events and the last twenty.

The seismic energy of the events of 2006 spans over five orders of magnitude. The distribution is bi-modal (see Fig. 6a), in agreement with the existence of two classes of events: If we estimate the distribution function separately for the two classes, we obtain two log-normal distributions that correspond to the two peaks of the bi-modal one (see Fig. 6c-d). Though the meaning of this frequency-energy distribution is very different from that of the seismic-tectonic framework (traditional b-value), it is interesting to look at the cumulative counts curve versus ε (for a detailed discussion see Rowe et al., 2000). The steeper portion of the curve (Fig. 6b) can be fitted by a straight line, whose slope ($\tilde{b}$) is approximatively 1.68. In other words, we have exploited the curve relatively to the energy ε to estimate $\tilde{b}$ whereas, usually, the b-value is obtained looking at the amplitudes. A simple transformation of variables allows to pass from the energy ε to the amplitude. So it results $b = 2(\tilde{b} - 1) \sim 1.4$, which is slightly different from that estimated for a different time period by Rowe et al. (2000).

Finally, we remark that the waveform class common to both 2005 and 2006 (second class) is composed of events with different energies in the two years, i.e. the explosions occurring in this class during 2006 are characterized by two orders of magnitude more energy than those of 2005.

5. Spectral properties

The high frequency energy of the explosions is mainly concentrated in the frequency range 1-8 Hz (see, e.g., Rowe et al., 2000), but a variety of spectra can be distinguished. Stacked spectra for the three waveform classes for 2005 and 2006 are reported in Figs. 7a-b, respectively.

The spectra appear different among the stations and between the three components of motion at the same station. In particular, the stacking of the spectra of the events of the first class shows a main peak at 3 Hz; the events of the second class (occurring both in 2005 and 2006) have two main peaks at 2 and 4 Hz. For the sake of completeness, we also report the stacked spectrum of the third class of events. Note again that they are uncorrelated

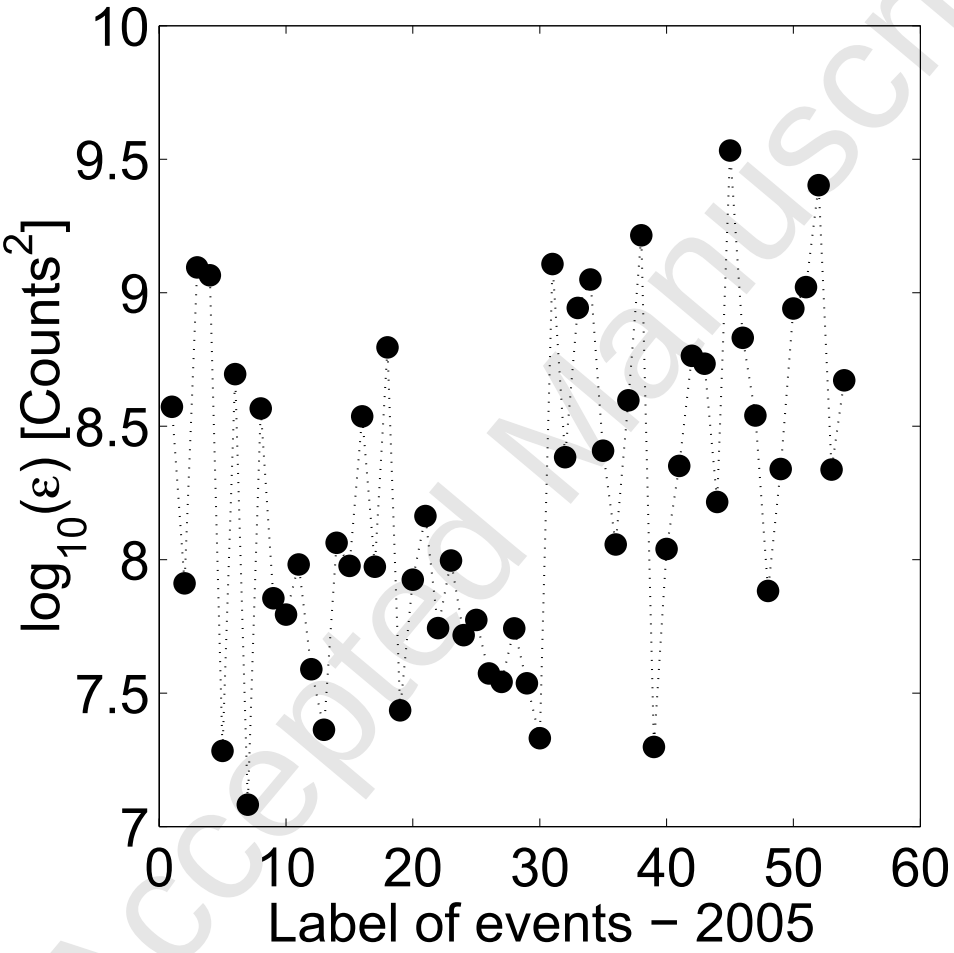

Figure 5: Curve of ε of the events recorded by E1S during 2005. The values are obtained by performing the Hilbert transform and integrating the square of the envelope of the radial seismic component of the explosions.

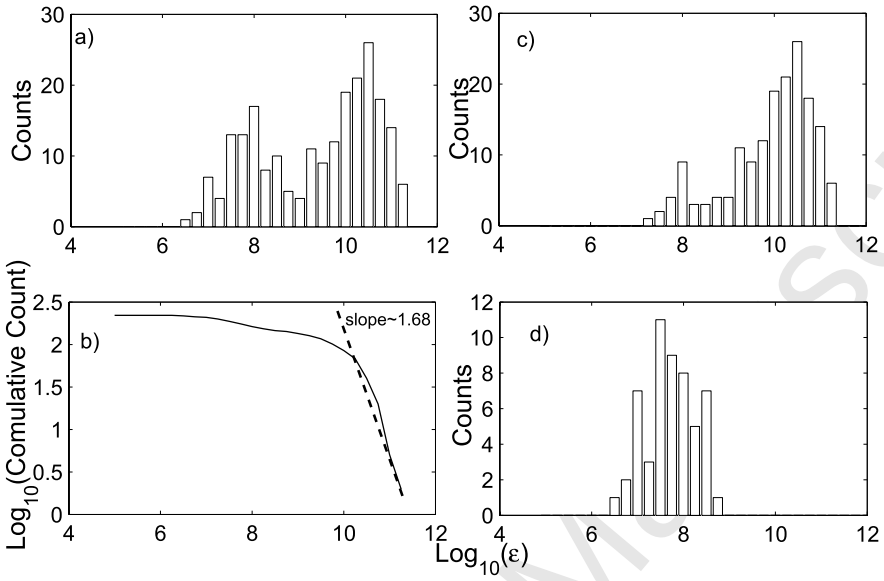

Figure 6: Distribution of ε of the explosions during 2006 (logarithmic scale) relative to the radial seismic component of E1S station: a) considering all the explosions two log-normal-like shapes appear; b) cumulative counts versus ε. The steeper portion can be fitted by a straight line. Focusing the attention on each class, the distributions of ε are log-normal-like both for the second c) and the third class d). Note that the superposition of these histograms perfectly match the overall distribution in a).

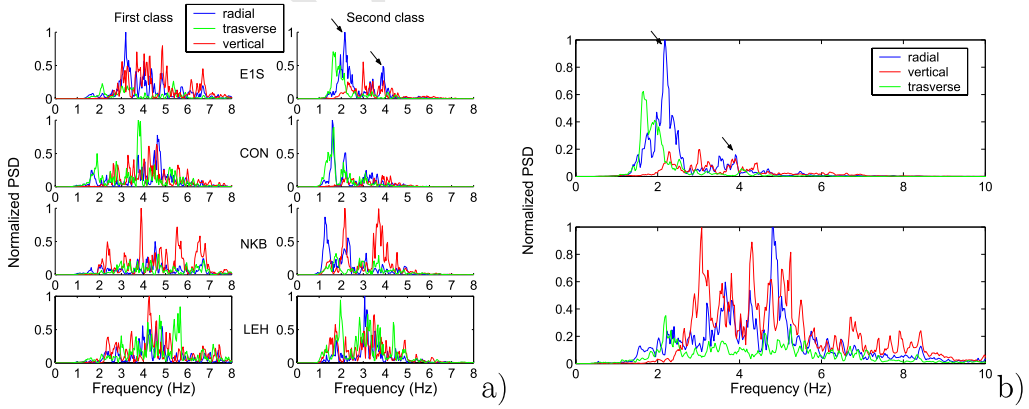

Figure 7: Normalized power spectra relative to: a) the two classes individuated in 2005; b) the events of the second class (upper panel) and third class (lower panel) recorded in 2006 by E1S.

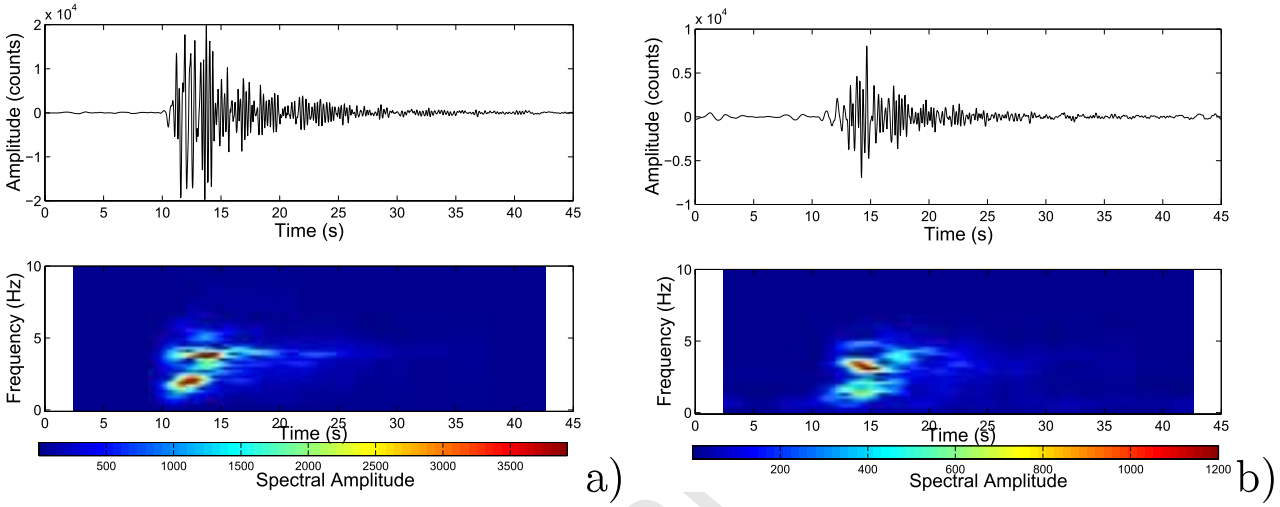

Figure 8: Waveform and spectrogram of the radial component of the event (27/02/05 h 23:40:24 UT) recorded at two stations: a) E1S and b) CON.

and this characteristic is reflected by a broad-band spectrum, which extends up to higher frequencies.

We focus our attention on the waveforms of the second class: the two spectral peaks correspond to two wavepackets, which appear to be shifted in time. An example of spectrogram analysis performed on a representative event recorded at E1S (located 704 m from the lava lake) is given in Fig. 8a: the 2 and 4 Hz main peaks in the spectrum are shifted in time and the lower frequency (2 Hz) precedes the higher (4 Hz). This analysis is performed on the same event recorded at CON (located 2 km from the lava lake). Stations E1S and CON are approximately aligned with the lava lake (see Fig.1), therefore the effects due to an anisotropic wavefield should be minimal. The results are reported in Fig. 8b. The delay between the arrival times of the wavepackets at CON is very short, so that the two wavepackets cannot be distinguished.

6. Infrasonic signals

The explosions at Erebus produce infrasonic waves that are recorded by two microphones located at stations E1S and NKB, 704 and 694 meters from the lava lake, respectively (Aster et al., 2003). Our data set contains the infrasonic data from 2005. The infrasonic signals have been studied

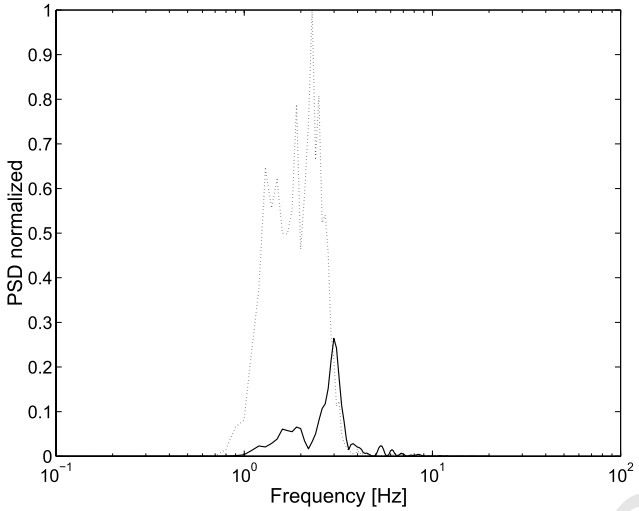

Figure 9: Normalized spectra relative to the infrasound recording, recorded by E1S. The signals show a frequency content in the range [1-3]Hz. Solid-line refers to an infrasound recorded on 07/02/2005 h 5:51:01 UT associated with a seismic event of the first class; Dotted-line refers to an infrasound recorded on 28/02/2005 at h 13:04:50 UT associated with a seismic event of the second class. Notice that in order to make a comparison, both spectra have been normalized with respect to the maximum amplitude of the infrasound recorded on 07/02/2005 h 5:51:01 UT.

extensively (see, e.g., Johnson et al., 2003). They show an impulsive onset produced by compression of the air, followed by quickly decaying oscillations (5-6 seconds), and are characterized by frequencies in the band 1-3Hz as illustrated in Fig. 9. The main peaks of the infrasound spectra coincide with the dominant frequencies of the corresponding radial seismic recordings at E1S (see, e.g., Fig. 7a). This is an indication that there is a common source process for the seismic and acoustic signals (De Lauro et al., 2007). The waveform analysis of infrasound signals shows clustering of events (see Fig. 10a) confirmed also by the energy distribution (see Fig. 10b): Two distinct classes of the explosions produce two distinct classes of infrasound signals.

The seismic/acoustic amplitude ratio is constant within 10% for each wavefield class, in agreement with the results of Rowe et al. (2000), who found that the ratio is constant for seismic amplitudes greater than 0.4 $\mu m/s$.

We note that the infrasonic signals in the first class of 2005 display an arrival time delay between stations E1S and NKB. This time delay is 0.30 $\pm$ 0.03s as indicated in Fig. 11a, and it disappears when the second class

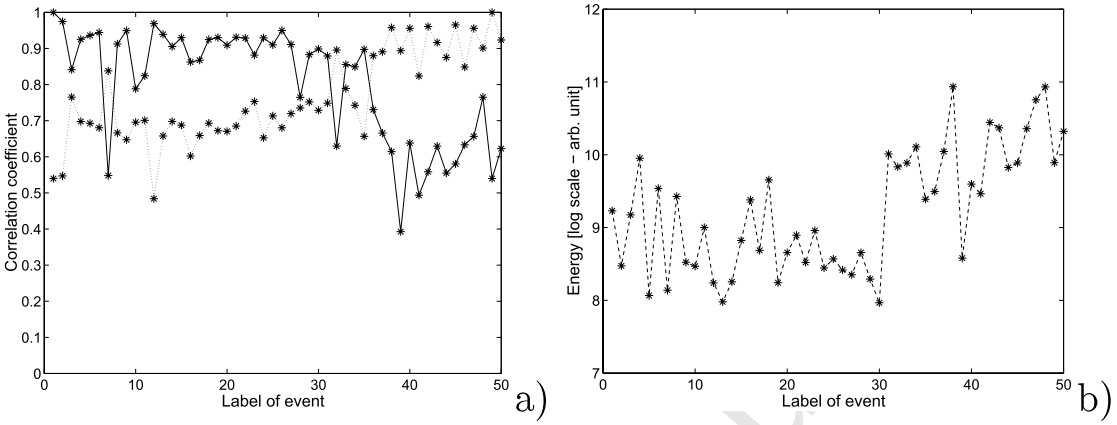

Figure 10: a)Cross-correlation curves relative to the infrasonic signals, which show clustering of events as in the case of seismic signals (the two reference events have been recorded on 07/02/2005 h 5:51:01 UT and on 25/02/2005 h 9:23:27 UT, respectively); b) the plot of a quantity proportional to the energy confirms the existence of the two classes.

of explosions is considered (see Fig. 11b). This delay cannot be observed in the seismic waveforms; probably because the seismic velocities are typically one order of magnitude higher than the sound velocity. This observed time delay is equivalent to a path length difference of about 100 m, suggesting that events in the first class emerge from different vent in the inner crater than the lava lake.

7. Polarization analysis

We perform a polarization analysis to investigate the incoming directions of the signals. The algorithm is based on the diagonalization of the covariance matrix of the three components of motion. The maximum eigenvector defines the polarization vector described by azimuth, dip and rectilinearity (RL). We take a reference frame defined by the East-West North-South plane and its normal (Vertical direction). The covariance matrices are computed on entire signals by selecting a sliding window of 1.5 s overlapped by 96% at every step, in order to obtain a significant statistics. The length of the window is chosen, as to contain a few cycles and thus to guarantee the stability of the solutions. The analysis is made on the whole data set on high-pass filtered signals with a corner frequency equal to 0.5 Hz. We shall describe the behavior of the polarization vector looking at its time-evolution and at averaged properties.

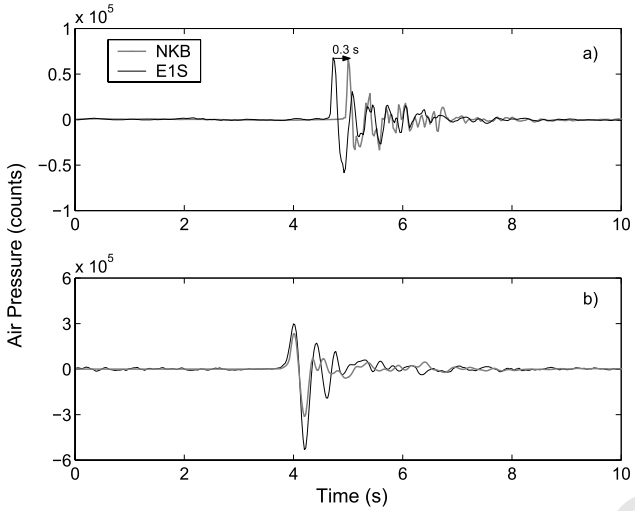

Figure 11: Infrasonic signals recorded at E1S and NKB: a) event recorded on 7/02/05 at 05:50:59 UT; b) event recorded on 28/02/2005 at 04:41:49 UT.

The polarization parameters have a general behavior independent of the waveform class and dependent on time. The results from station E1S for the three extracted waveform classes are reported in Fig. 12. At E1S the radial component (in the direction of lava lake) makes an angle N57.9^{o}E. We observe azimuths pointing towards the lava lake and high rectilinearity ($RL > 0.7$); the dip parameter assumes high values for a few seconds at the onset of the explosion (eigenvector almost parallel to the plane NS-EW), then it becomes steeper and reaches a relatively stable value around 40^o. The particle motions of the stacked explosions of Fig. 13 clearly illustrate this steepening of the dip, in agreement with previous results from VLP analyses (Rowe et al. 1998, 2000).

The analysis of the signals recorded by the other stations (in 2005) shows a different behavior. For example, at station NKB, located at the same distance from the crater area as E1S, the values of RL are lower (~ 0.6), and the azimuths are not well defined. The signal-to-noise ratio appears to be lower than at E1S. However, some dominant peaks can emerge from the distributions of the polarization parameters computed considering all the explosions of every class, allowing a comparison between the two stations E1S and NKB. The results of the polarization analysis for the events of the first class are shown in Figs. 14-15. Looking at E1S (Fig. 14a-c), almost all

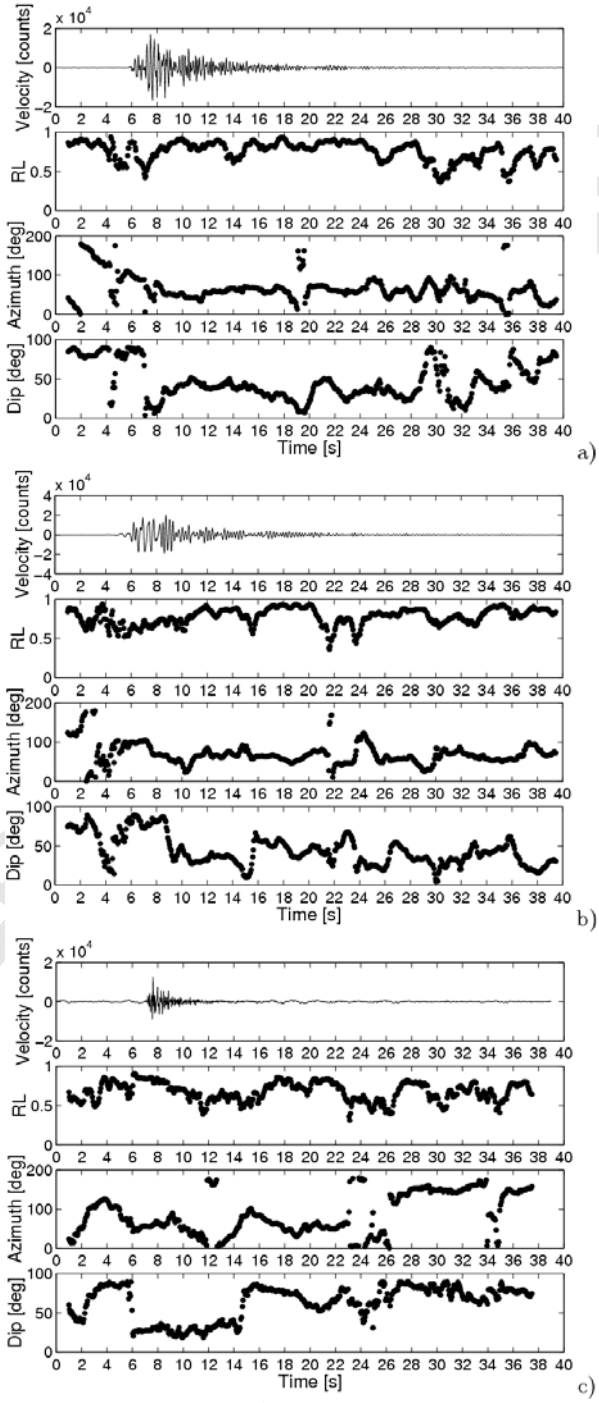

Figure 12: Time evolution of the polarization parameters of the seismic signals computed on windows 1.5s long, sliding 0.06s every step: a) An example of the first class recorded on 07/02/2005 h 05:50:56 UT; b) An example of the second class recorded on 02/07/2005 h 23:40:28 UT; c) An example of the third class recorded on 12/03 h 15:21:29 UT. The plotted waveforms are relative to the radial component at E1S

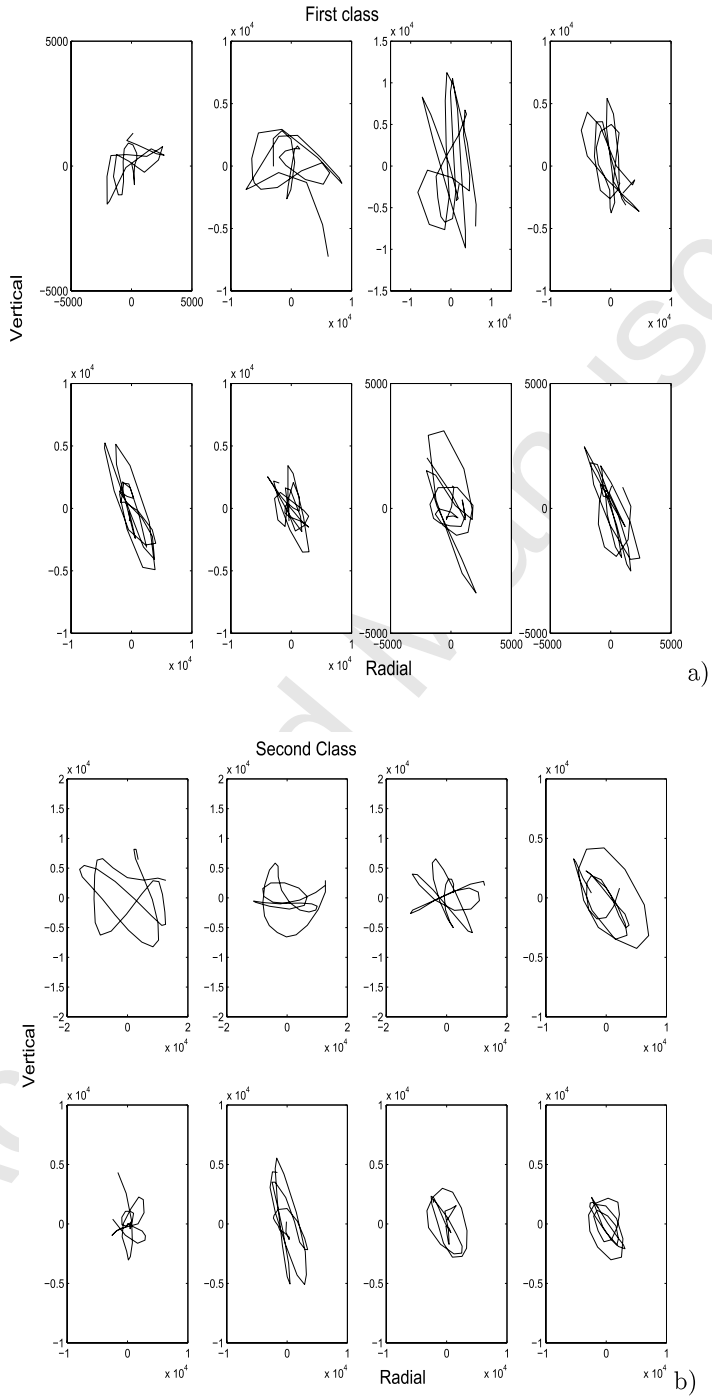

Figure 13: Particle motion at station E1S relative to the stacked explosion: a) first class; b)second class. Each frame is *one* second long starting from the onset of the explosion. The onset is shallow, then the dip reaches approximately 40^o.

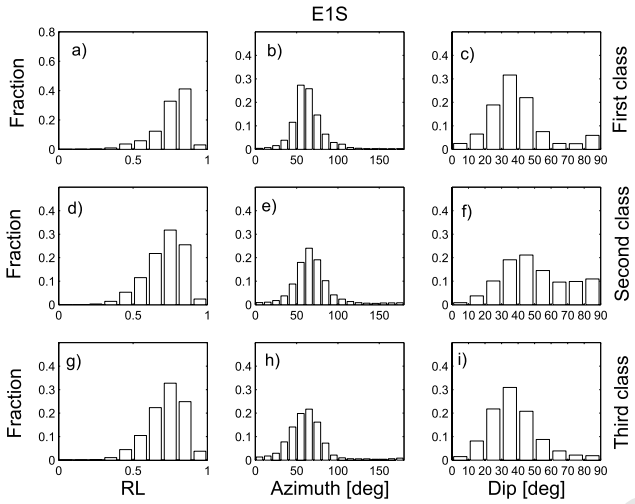

Figure 14: Mean distributions of the polarization parameters for the three classes of events at E1S (2005 and 2006). (a),(b),(c): distribution of rectilinearity, azimuths and dip angles of the first 20 seconds of the events of the first class. Identically, (d),(e),(f) correspond to the events of the second class and (g),(h),(i) to the events of the third class. Note that the general properties are shared.

the solutions show high values of RL (greater than 0.7); the distribution of the azimuths is peaked at the angle pointing towards the lava lake, and the dips are mainly grouped between 30^o-40^o. Looking at NKB (Fig. 15a-c), the values of RL are on average smaller than at E1S; the azimuths indicate radial directions and the dips are between 10^o-30^o. Regarding the second class of events at E1S (Fig. 14d-f), we observe azimuths with a dominant peak in the direction of the crater area with high values of RL. The distribution of the dips is enriched in shallow values. The distributions for NKB show similar characteristics (Fig. 15d-f). Finally, regarding the third class, with respect only to E1S (Fig. 14g-i) the properties found in the previous cases are preserved on average. For the second class of events, the contribution of the dips $> 50^o$ is significant and comes from frequencies ≤ 2 Hz: The onset is shallow. Finally, we note small difference between the azimuths of the first class ($50^o - 60^o$) and those of the second class ($60^o - 70^o$). This is another indication that the two classes are associated with different vibrating structures.

The results of the polarization analysis at stations CON and LEH do not yield stable solutions, nor distributions, even considering the stacking of

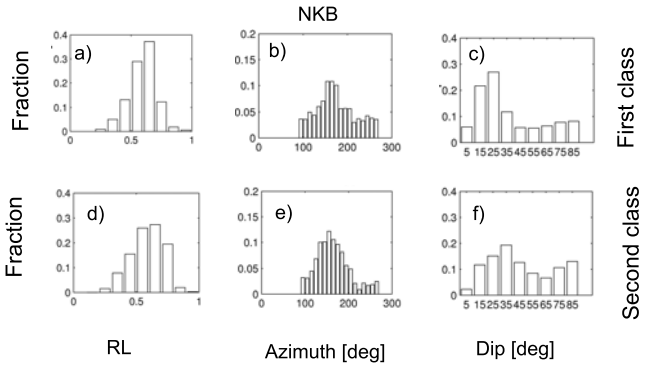

Figure 15: Mean distributions of the polarization parameters for the two classes of events at NKB (2005). (a),(b),(c): Distribution of rectilinearity, azimuths and dip angles of the first 20 seconds of the events of the first class. Identically, (d),(e),(f) correspond to the events of the second class. Note that the general properties are shared.

aligned events in the same class. In fact, RL is generally less than 0.5 and the angle parameters lose their significance.

8. Summary of seismological setting

Previous analyses show the existence of three classes of events distinct in waveform and energy but with similar average polarization properties. The comparison of the acoustic and seismic signals allows us to infer that the first and the second classes of events emerge from different vents spaced about 100 m. Two distinct phases of the volcanic activity are observable: The first, non stationary, is characterized by an intense clustered activity composed of events from class 1 occurring in a single day of 2005, and evolving towards the events from class 2; the second along 2006 with a stationary behavior is mainly characterized by events from class 2. The observed variety of waveforms is basically associated with the different vibrating structures excited, although all localized within the crater area. The non stationary phase might have been triggered by phenomena, which are often observed on this volcano as, for instance, wasting of rock, snow and ice from the crater walls (Rowe et al., 2000). In any case, the formation and the ascent of bubbles is, in both cases, the cause of observed vibrations.

In the following macroscopic analysis, performed in order to extract basic properties of the formation, growth, ascent, bursting of bubbles, we shall primarily concentrate our attention on the stationary phase. This corresponds

to the analysis carried out for Stromboli. Furthermore, we extract some properties, which can have a more general meaning shedding light also on the non stationary phase.

9. Macroscopic behavior of Erebus volcano

The analyses of the previous sections confirm and improve many of the results obtained by looking at Erebus explosive activity along different time periods and different portions of the spectrum (see, e.g., Aster at al. 2003; Rowe et al. 1998, 2000). They establish the seismic wavefield properties on the time-scale of the explosions' duration. To get an overall comprehension of the explosion generating process, we study the macroscopic behavior of Erebus volcano on longer time-scale. Specifically, we investigate the distribution of inter-explosion times, whose occurrence will be described by a dynamic model providing intermittency. A statistically well supported analysis requires a suitable data base. For this reason we apply our analysis only to the events of 2006.

9.1. Analysis of inter-explosion times

The distribution function of the inter-explosion times contains significant information on the dynamic process generating the exploding gas bubbles. A qualitative analysis could lead to the hypothesis that the occurrence is a periodic phenomenon. A more careful observation may reveal the existence of significant fluctuations of the times between successive explosions, as happens at Stromboli (Bottiglieri et al., 2005). The macroscopic quantity to be considered is the square of the maximum amplitude of the explosions as reported in Fig. 16a.

The inter-explosion times (Δt) are the difference of the occurrence times of two successive maxima; their evolution is reported in Fig. 16b along with the relative distribution (Fig. 16c). A very clear exponential shape can be seen. As is well known, an exponential distribution is typical of a Poissonian behaviour (Cox and Lewis, 1966). The fit of the data allows the estimation of the average time interval between explosions $\frac{1}{\lambda} = 5.5$ hours, which is the rate of the Poissonian process. We perform a standard test to check the Poissonian behaviour of a distribution, i.e., we evaluate the variability coefficient defined as:

$$C_V = \frac{\sigma_{\Delta t}}{\overline{\Delta t}}, \tag{1}$$

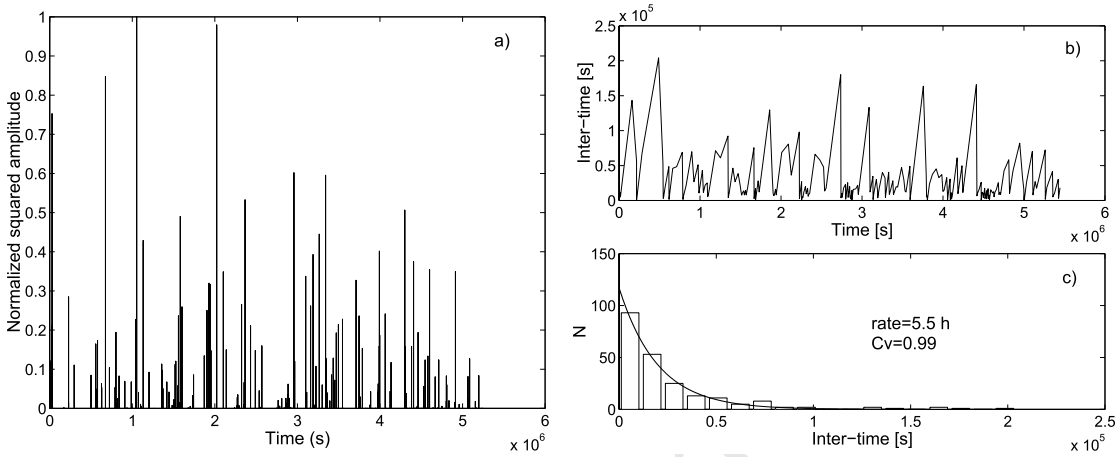

Figure 16: a) Evolution of the squared amplitude of the explosions at Erebus in the selected period of 2006; b) Inter-time evolution and c) distribution, which reveals the existence of a Poisson process underlying the generation of the exploding gas bubbles.

where $\sigma_{\Delta t}$ is the standard deviation and $\overline{\Delta t}$ is the mean value of the inter-times. We have $C_V = 1$ for a Poissonian process, whereas $C_V > 1$ is for a clustered process and $C_V = 0$ is for a periodic one. The limit $C_V \to \infty$ indicates an uniform distribution. For Erebus explosions C_V is equal to 0.99, confirming that the occurrence of the explosions is driven by a Poisson process. The same result was obtained at Stromboli, i.e. the explosion occurrence is ruled by a Poissonian process whose rate, obviously different, is about 3 min (Bottiglieri et al., 2005).

9.2. Intermittency

The Poissonian occurrence of the explosions at Erebus can be described by a dynamic model providing classical intermittency as for Stromboli (Bottiglieri et al., 2008).

Intermittency is a phenomenon observed in a variety of physical systems; specifically, they appear quiescent for long periods with sudden bursts of activity. The phenomenon was first observed by Batchelor and Townsend (1949) looking at a fluctuating velocity field in fully developed turbulence. The switch between bursts and the quiescent state appears to occur randomly. In the last few years many models have been produced and a variety of mechanisms has been explored. The intermittent model provides a coarse grained description of the system on the time scale of the explosions' oc-

currence. In this conceptual scheme, a suitable coarse-grained variable is the maximum amplitude of the explosion quakes or equivalently its square (proportional to the energy).

We introduce the modified general (two-dimensional) map of Venkataramani et al. (1996) with representative variables x and y:

$$\begin{aligned} x_{n+1} &= 2r_n x_n \mod 1 \\ y_{n+1} &= [\lambda(x_n, p) y_n + \epsilon y_n^{\sigma} + q\cos(2\pi \mathrm{x_n})]_*, \end{aligned} \tag{2}$$

where $\epsilon = \pm 1$, $\lambda(x_n, p) = p + \cos(2\pi \mathrm{x_n})$, σ is the lowest order of nonlinearity, $r_n = 1$ if $x_n < 0.5$ and r_n is a random value when $x_n \geq 0.5$, p is the bifurcation parameter characterizing the strength of the coupling. The function $[\cdot]_*$ is defined as follows: $[\eta]_* = \eta$ if $|\eta| \leq 1$ and $[\eta]_* = \eta - 1.5\mathrm{sgn}(\eta)$ if $|\eta| > 1$; this provides a simple confining nonlinearity. We have modified Venkataramani et al. (1996)'s map introducing r_n that takes random values in the uniform distribution in order to avoid the fixed point of the *tent* map, $x_{n+1} = 2r_n x_n \mod 1$. In mathematics, the *tent* map is an iterated function, in the shape of a tent, forming a discrete-time dynamical system. It takes a point x_n on the real line and maps it to another point x_{n+1}. Depending on the value of r_n, the *tent* map provides a range of dynamical behaviour from predictable to chaotic. We choose the Venkataramani et al.(1996)'s map because it retains the most significant aspects necessary to produce intermittency, i.e. a simple confining nonlinearity and the Poissonian occurrence of the explosions such as that found at Erebus.

Numerically, we construct a time series taking the square of the maximum amplitude of the explosion quakes as reported Fig. 16a (for a detailed description see Bottiglieri et al., 2008). Our intermittency model (Eq. 2) should reproduce the evolution of this series, once recognized x_n as an effective time and y_n the maximum amplitude.

From the comparison between the square of the maximum amplitude of the explosions and y_n^2, the best choice for the parameters of map (Eq. 2), in the sense of the least squares, is $\epsilon = 1$, $p = 0.2$, $q = 0.016$ and $\sigma = 2$. Fig. 17a shows the corresponding simulated map. A suitable amplitude threshold is fixed to avoid map-generated noise. The inter-explosion time distribution of the extracted simulated peaks is reported in Fig. 17b. The exponential shape is preserved as well as the rate of the Poissonian process. This implies successful modelling.

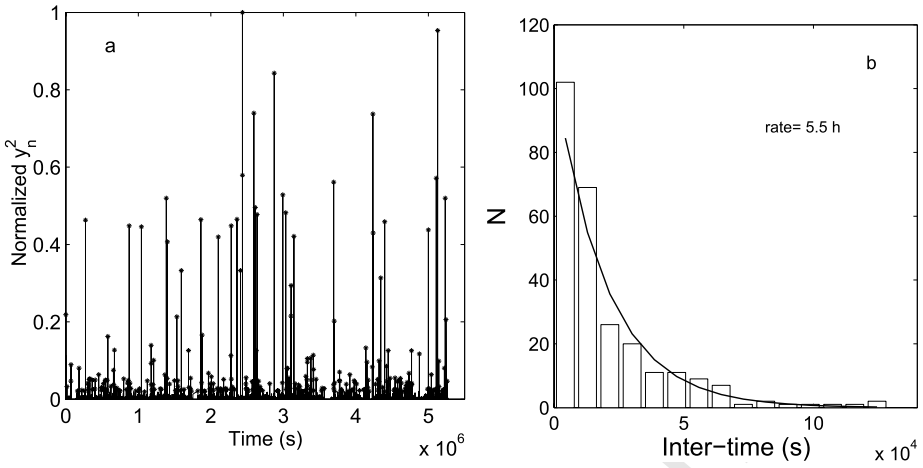

Figure 17: a) Normalized squared amplitude of the simulated map as function of time. The asterisks denote individual peaks above the threshold equal to 0.015; b) Inter-time distribution of the simulated map. The exponential shape of the distribution suggests a Poissonian process whose estimated rate of about 5 hours is in agreement with the experimental rate of the explosion occurrence at Erebus during 2006.

10. Chandrasekar-Landau model for large gas bubble formation

The above results indicate that Erebus displays a behavior similar to Stromboli, i.e. Poissonian occurrence of the explosions and an intermittent phenomenon explaining the alternation between quiescent states and bursts of activity, but on different time scales. This similarity leads us to consider the Chandrasekar-Landau model to describe the gas slug formation (Chandrasekar, 1943; Bottiglieri et al., 2005). This mean-field model of coalescence considers the growth from aggregation induced by diffusion of little bubbles. Erebus' degassing activity is described in, e.g., Oppenheimer and Kyle (2008). For stationary phase, the coalescence model added to the inter-explosion time distribution allows to infer the distribution of the gas bubble sizes.

Here, we assume that coalescence is the generating mechanism of the explosive bubbles. Let us take two elementary bubbles: they diffuse in the melt and when they meet they coalesce. The diffusive dynamics implies the following kinematic relation between the distance x and the time t through a diffusion coefficient D:

$$x^2 = D \cdot t. \tag{3}$$

Coalescence implies dynamical scaling and, therefore, the existence of a characteristic length scale L and of a scaling parameter α. Hence, the space interval x, travelled by two elementary constituents to get into contact, is proportional to L. The diffusion coefficient scales with L as

$$D = D_o \left(\frac{L_o}{L} \right)^{\alpha}, \tag{4}$$

where L_o is the length of the nucleating elementary constituents and D_o is the associated diffusion coefficient. The N step process is simply obtained by using the sum rule of Gauss (Chandrasekar, 1943) and provides the coalescence time:

$$\frac{N(N+1)}{2} \Delta t_c = \frac{L^{\alpha+2}}{D_o L_o^{\alpha}}, \tag{5}$$

where Δt_c is the coalescence time, i.e, the inter-explosion times. Assuming that the ascent process of the exploding bubbles is simply driven by buoyancy, the ascent time can be considered constant and the inter-explosion time distribution becomes:

$$f(\Delta t_c) = \lambda e^{-\lambda \Delta t_c}. \tag{6}$$

By a standard transformation of variables on the inter-explosion distribution function, we can derive the distribution function for the gas bubbles' size:

$$F(L) = \lambda \cdot A(\alpha + 2) \cdot L^{\alpha+1} \cdot e^{-\lambda A L^{\alpha+2}}, \tag{7}$$

where

$$A = \frac{1}{L_o^{\alpha} D_o N(N+1)/2}. \tag{8}$$

Notice that the coefficients D_o, N and L_o scale proportionally and $\alpha = 1 + \frac{1}{d}$, where d is the topological dimension (Gunton, 1983).

We assume typical values for D_o, L_o and N (see e.g. Dibble, 1994; Cardoso et al., 1999; Blower et al., 2003) as reported in the legend of Fig. 18; λ is the explosion occurrence rate i.e. $\frac{1}{\lambda} = 5.5\ h$. The resulting distribution functions are shown in Fig. 18 for the topological dimension $d = 2, 3$. For all the ranges of parameters, the most probable size is peaked around the order of magnitude of meters. Note that the curves with $d = 3$ better recover the variability in sizes reported in the literature (Johnson and Aster, 2005). This observation leads us to hypothesize that the gas bubbles

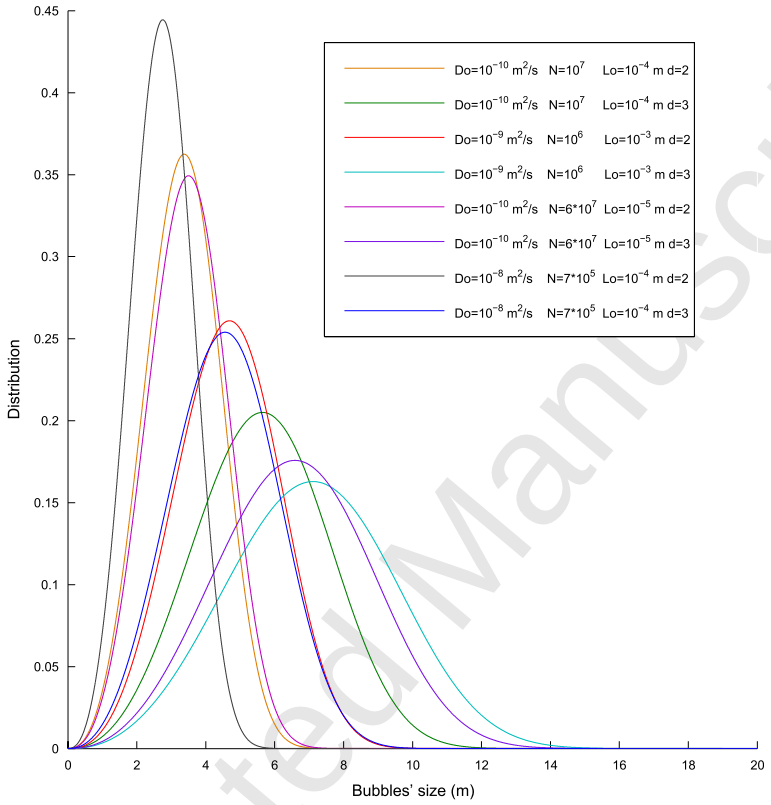

Figure 18: Distribution functions of the bubbles' size as derived by Chandrasekar-Landau model: the model provides coalescing bubbles size of a few meters.

are more similar to a sphere than a slug as shown by the video observations reported in Aster et al. (2004) and displayed on the MEVO website (http://erebus.nmt.edu/video/eruptions_stromb.html). It is interesting to observe that, at Stromboli, slug geometry (i.e. d=2) better describes the observed sizes; the shape of the exploding gas bubbles appears to have a non-trivial relation with the volcanic edifice.

11. A simple model of ascent of gas bubbles

Diffusion can be considered a basic mechanism acting within the magma (see, e.g., Gonnermann and Manga, 2007), and our model shows that it appears to play a significant role in the formation of large bubbles. In this section, we generalize the classical equation for ascent of gas bubbles, introducing Brownian fluctuations. As it is well known, the classical dynamics are governed by gravity, buoyancy and Stokes' law that takes into account viscous effects. On this basis, the dynamics of a spherical bubble can be represented by the stochastic differential Ito equation:

$$dv = \left(-\gamma v + \frac{Vg(\rho_f - \rho_g)}{m}\right) dt + \gamma\sqrt{2\tilde{D}}dw; \gamma = \frac{6\pi R\nu}{m}, \tag{9}$$

where dw is the standard Wiener process, v is the velocity, $\tilde{D}$ is an effective diffusion coefficient, g is the gravity acceleration, R, V, m are respectively the radius, the volume, and the mass of the gas, ρ_f and ρ_g are the density of the fluid and the density of the gas bubble, and ν is the viscosity.

The Ito equation implies the Fokker-Planck equation for transition probability P (see, e.g., Risken 1996):

$$\frac{\partial P(v,t)}{\partial t} = -\frac{\partial v_+(v,t)P(v,t)}{\partial v} + \tilde{D}\frac{\partial^2 P(v,t)}{\partial^2 v}, v_+ = \gamma v - \frac{Vg(\rho_f - \rho_g)}{m}. \tag{10}$$

The stationary solution is

$$P(v) = \sqrt{\frac{1}{2\pi\gamma\tilde{D}}} \exp\left(-\frac{\left[v - \frac{Vg(\rho_f-\rho_g)}{6\pi R\nu}\right]^2}{2\tilde{D}\gamma}\right). \tag{11}$$

Notice that the mean value of the velocity corresponds to the classical value in the asymptotic regime, which is given by the ratio between the buoyancy and the viscous effects. This implies that larger bubbles experience larger velocities.

Velocity is influenced by two terms:

- the mean value $\frac{Vg(\rho_f-\rho_g)}{6\pi R\nu}$;
- the fluctuations ($\sqrt{\gamma\tilde{D}}$).

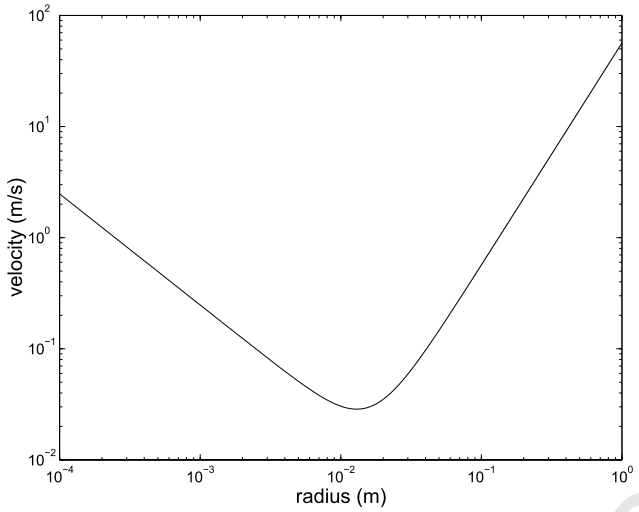

Figure 19: Estimation of velocity as a function of the bubbles' radius, combining diffusive and gravity effects. As can be seen, up to a radius of a few millimeters, diffusion is dominant (and favors coalescence), whereas buoyancy becomes relevant for bubbles with radius larger than a few centimeters.

These two terms depend on the size of the bubble. We can estimate the relevance of the two terms by considering: The basaltic magma viscosity $\nu = 100$ Pa$\cdot s$; $\tilde{D} = 1.5 \times 10^{-10}\ m^2/s$; $\rho_f = 2600\ kg/m^3$ and $\rho_g = 1.1\ kg/m^3$ (Dibble, 1994).

These calculations confirm that the size of the bubbles plays an important role in the dynamics as shown in Fig. 19. In fact for small radii (up to a few millimeters) the dynamics are ruled by diffusion. However, the velocities induced by this term are quite small ($\sim$ 1 m/s) and the gas bubbles are confined and coalescence is favored. On the contrary, for large radii (on the order of centimeters), diffusion can be neglected and the bubbles rise with the limit velocity. For a radius of 1 m, this velocity is $\sim$ 50 m/s in a basaltic magma.

12. Conclusions

We have analyzed seismic signals associated with the explosion quakes at Erebus volcano (Antarctica) in two time periods from 2005 and 2006. By cross-correlation analysis, we have identified three classes of events, one of which occurs both in 2005 and 2006. The first class of 2005 appears to be

clustered in time. The second class (both in 2005 and 2006) is characterized by a spectrum with two dominant peaks. The events of the third class, recorded only in 2006, display a variable frequency content, with relevant peaks up to 5 Hz. This class is essentially made of events, which are uncorrelated both with the other classes and among themselves. The distributions of a quantity proportional to the energy reveal a log-normal behavior for all the classes. The explosions of the second class occurring during 2006 are characterized by two orders of magnitude more energy than in 2005. Polarization analysis of the high frequency portion of the spectrum of the explosions indicates radial incoming directions of the wavefield in agreement with Rowe et al. (2000) considering VLP signals, suggesting a persistent shallow source.

Two distinct phases of volcanic activity are evidenced: The first (2005) with accelerated bubbles formation and evolving to a stationary phase, the second (2006) characterized by stationarity. The macroscopic analysis has been performed looking at the stationary phase.

We hypothesize that the transition between small and large gas bubbles can be described by a coalescence phenomenon driven by a diffusion process. In fact, the standard Chandrasekar-Landau mean-field model is able to provide the observed bubble sizes. Similar to Stromboli, even though on a different time scale, we observe at Erebus a Possonian inter-explosion times, with a rate of about 5.5 hours in comparison to the 3-4 min found at Stromboli by Bottiglieri et al. (2005), and the transition between quiescent states and bursts of activity can be described by a low-dimension dynamic system in an intermittent regime.

Finally, the classical equation of the ascent gas bubble dynamics is generalized introducing a diffusive term. This yields a Fokker Planck equation, whose stationary solution depends on the gas bubbles' radius: for a radius up to a few millimeters, diffusion dominates the dynamics. The gas bubbles are confined, making coalescence favored. For a radius of the order of 10 cm, buoyancy becomes dominant and the bubble velocity rapidly increases with the radius.

We remark that high frequency ($> 0.5Hz$) tremor is completely lacking at Erebus in the investigated period, whereas it is the persistent ground motion observed at Stromboli (De Lauro et al., 2008). Generation of volcanic tremor likely requires an abrupt expansion of flow that self-interacts through an impingement (Villermaux and Hopfinger, 1994). This condition is verified at Stromboli that is characterized by a conic-like conduit, while it could not be compatible with the volcanic edifice at Erebus. In any case, tremor

signals could occur beneath the sensitivity threshold given by the ambient background noise. In addition, the appearance of tremor could be prevented because of the strong acoustic isolation of the shallower part of the lake by which the smaller bubbles are not able to communicate the seismic energy to the seismic stations as conjectured by Rowe et al. (2000).

In conclusion, the Strombolian stationary phase of Erebus volcano presents many of the characteristics observed at Stromboli, even though on a longer time scale (Bottiglieri et al., 2005; De Lauro et al., 2008).

As a final remark, we underline that the coalescence model (Eqs. 3-5) and the ascent of gas bubble equation are associated with the formation, growth and dynamics of the gas bubble, therefore they are applicable to stationary as well as non-stationary phases. On the contrary, the occurrence in time of bubbles, and the associated intermittent model can be appropriate to describe only the stationary phase. This suggests that the physics involved in the gas bubble ascent and in the coalescence process drives the behavior of volcanoes displaying Strombolian-like activity.

References

[1] Aster, R., S. Mah, P. Kyle, W. McIntosh, N. Dunbar, J. Johnson, M. Ruiz, and S. McNamara (2003), Very long period oscillations of Mount Erebus Volcano, *J. Geophys. Res.*, *108*,B11, 2522, doi:10.1029/2002JB002101.

[2] Aster, R., W. Mcintosh, P. Kyle, R. Esser, B. Bartel, N. Dunbar, B. Johns, J. Johnson, R. Karstens, C. Kurnik, M. Mcgowan, S. Mcnamara, C. Meertens, B. Pauly, M. Richmond, and M. Ruiz (2004), Real-time Data received from Mount Erebus volcano, Antarctica, *EOS*, *85*, 97–104.

[3] Batchelor, G. K., and A. A. Townsend (1949), The nature of turbulent motion at large wave-numbers, *Proc. R. Soc. London, Ser. A*, *199*, 238–255.

[4] Blower, J. D., J. P. Keating, H. M. Mader, and J. C. Phillips (2003), The evolution of bubble size distributions in volcanic eruptions, *J. Volcanol. Geotherm. Res.*, *120*, 1–23.

[5] Bottiglieri, M., S. De Martino, M. Falanga, C. Godano, and M. Palo (2005), Statistics of inter-time of Strombolian explosion-quakes, *Europhys. Lett.*, *72*, 492–498.

[6] Bottiglieri, M., S. De Martino, M. Falanga, and C. Godano (2008), Strombolian volcanic activity as an intermittent phenomenon, *Europhys. Lett.*, *81*, 49001, doi:10.1209/0295-5075/81/49001.

[7] Cardoso, S. S., and A. W. Woods (1999), On convection in a volatile-saturated magma, *Earth and Planet. Sci. Lett.*, *168*, 301–310.

[8] Chandrasekhar, S. (1943), Stochastic problems in physics and astronomy, *Rev. of Mod. Phys.*, *15*, 1–89.

[9] Cox, D. R., and P. A. Lewis (1966), *The statistical analysis of series of events*, Metuen, London.

[10] De Lauro, E., S. De Martino, M. Falanga, A. Ciaramella, R. Tagliaferri (2005), Complexity of time series associated to dynamical systems inferred from independent component analysis, *Phys. Rev. E*, *72*, 046712, 2005.

[11] De Lauro E., S. De Martino, M. Falanga, M. Palo, Analysis of Erebus Volcano and its comparison with Stromboli,IUGG XXIV, Perugia, 2007.

[12] De Lauro, E., S. De Martino, E. Del Pezzo, M. Falanga, M. Palo, and R. Scarpa (2008), Model for high frequency Strombolian tremor inferred by wavefield decomposition and reconstruction of asymptotic dynamics, *J. Geophys. Res.*, *113*, B02302, doi:10.1029/2006JB004838.

[13] De Martino, S., M. Falanga, and C. Godano (2004), Dynamical similarity of explosions at Stromboli Volcano, *Geophys. J. Int.*, *157*, 1247–1254, doi:10.1111/j.1365-246X.2004.02263.x.

[14] Dibble, R.R. (1994), *Velocity modeling in the erupting magma column of Mount Erebus, Antarctica*, in Volcanological and Environmental Studies of Mount Erebus, Antarctica, edited by P.R. Kyle, pp. 17–33, American Geophysical Union.

[15] Giggenbach, W., P. Kyle, and G. Lyon (1973), Present volcanic activity on Mt. Erebus, Ross Island, Antarctica, *Geology*, *1*, 135–156.

[16] Gonnermann, H. M., and M. Manga (2007), The fluid mechanics of volcanic eruptions, *Ann. Rev. Fluid. Mech.*, *39*, 321–356.

[17] Gunton J. D., M. San Miguel, and P. S. Sahni (1983), *Phase Transitions*, edited by Domb-Green, 8, Academic Press, London.

[18] Johnson, J., M. Lees, M. Ruiz, P. McChesney, R. Aster, and P. Kyle (2003), Interpretation and utility of infrasonic records from erupting volcanoes, *J. Volcanol. Geotherm. Res.*, *121*, 1563.

[19] Johnson, J.B., and R. C. Aster (2005), Relative partitioning of acoustic and seismic energy during Strombolian eruptions, *J. Volcanol. Geotherm. Res.*, *148*, 334–354.

[20] Kaminuma, K. (1987), Seismic activity of Erebus volcano, Antarctica, *Pure and Applied Geophysics*, *125*, 993–1008, doi:10.1007/BF00879364.

[21] Konstantinou, K. I. (2002), Deterministic non-linear source processes of volcanic tremor signals accompanying the 1996 Vatnajoökull eruption, central Iceland, *Geophys. J. Int.*, *148*, 663–675.

[22] Kyle, P. (1977), Mineralogy and glass chemistry of volcanic ejecta from Mt. Erebus, Antarctica, *N. Z. J. Geol. Geophys.*, *20*, 1123-1146.

[23] Kyle, P. R., J. A. Moore, and M. F. Thirlwall (1992), Petrologic evolution of anorthoclase phonolite lavas at Mount Erebus, Ross Island, Antarctica, *J. Petrology*, *33*, 849–875.

[24] Maurel, A., P. Ern, B. J. A. Zielinska, and J. E. Wesfreid (1996), Experimental study of self-oscillations in a confined jet, *Phys. Rev. E*, *54*, 3643–3651.

[25] Oppenheimer, C., and P. R. Kyle (2008), Probing the magma plumbing of Erebus volcano, Antarctica, by open-path FTIR spectroscopy of gas emissions, *J. Volcanol. Geotherm. Res.*, in press.

[26] Risken H., The Fokker-Planck Equation: Methods of Solution and Applications (1996), Springer-Verlag, Berlin.

[27] Rowe, C., R. Aster, P. Kyle, J. Schlue, and R. Dibble (1998), Broadband recording of Strombolian explosions and associated very-long-period seismic signals on Mount Erebus Volcano, Ross Island, Antarctica, *Geophys. Res. Lett.*, *25*, 2297–2300.

[28] Rowe, C. A., R. C. Aster, P. R. Kyle, R. R Dibble, and J. W. Schulue (2000), Seismic and acoustic observations at Mount Erebus Volcano, Ross Island, Antarctica, *J. Volcanol. Geotherm. Res.*, *101(12)*, 105–128.

[29] Rowe, C. A., C. H. Thurber, and R. A. White (2004), Dome growth behavior at Soufriere Hills Volcano, Montserrat, revealed by relocation of volcanic event swarms, 1995-1996, *J. Volcanol. Geotherm. Res.*, *134 (3)*, 199–221.

[30] Shibuya, K., R. R. Dibble, M. Baba, and P. R. Kyle (1989), *Classification of volcanic earthquakes at Mount Erebus, Antarctica*, J. Latter, ed., Volcanic Hazards, assessment and monitoring, Springer-Verlag, Berlin, 520–535.

[31] Venkataramani, S. C., Hunt, B. R., and E. Ott (1996), Transition to Bubbling of Chaotic Systems, *Phys. Rev. Lett.*, *77*, 5361.

[32] Villermaux, E., and E. J. Hopfinger (1994), Self-sustained oscillations of a confined jet: a case study for non-linear delayed saturation model, *Physica D*, *72*, 230–243.